

Article

Radiation-Free Microwave Technology for Breast Lesion Detection Using Supervised Machine Learning Model

Soumya Prakash Rana ^{1,*}, Maitreyee Dey ¹, Riccardo Loretoni ², Michele Duranti ³, Mohammad Ghavami ¹, Sandra Dudley ¹ and Gianluigi Tiberi ^{1,4}

¹ School of Engineering, London South Bank University, London SE1 0AA, UK

² Breast Screening and Diagnostic Breast Cancer Unit, AUSL Umbria 2, 06034 Foligno, Italy

³ Department of Diagnostic Imaging, Perugia Hospital, 06156 Perugia, Italy

⁴ Umbria Bioengineering Technologies (UBT) Srl, 06081 Perugia, Italy

* Correspondence: soumyaparakash.rana@gmail.com or ranas11@lsbu.ac.uk

Abstract: Mammography is the gold standard technology for breast screening, which has been demonstrated through different randomized controlled trials to reduce breast cancer mortality. However, mammography has limitations and potential harms, such as the use of ionizing radiation. To overcome the ionizing radiation exposure issues, a novel device (i.e. MammoWave) based on low-power radio-frequency signals has been developed for breast lesion detection. The MammoWave is a microwave device and is under clinical validation phase in several hospitals across Europe. The device transmits non-invasive microwave signals through the breast and accumulates the backscattered (returned) signatures, commonly denoted as the S_{21} signals in engineering terminology. Backscattered (complex) S_{21} signals exploit the contrast in dielectric properties of breasts with and without lesions. The proposed research is aimed to automatically segregate these two types of signal responses by applying appropriate supervised machine learning (ML) algorithm for the data emerging from this research. The support vector machine with radial basis function has been employed here. The proposed algorithm has been trained and tested using microwave breast response data collected at one of the clinical validation centres. Statistical evaluation indicates that the proposed ML model can recognise the MammoWave breasts signal with no radiological finding (NF) and with radiological findings (WF), i.e., may be the presence of benign or malignant lesions. A sensitivity of 84.40% and a specificity of 95.50% have been achieved in NF/WF recognition using the proposed ML model.

Keywords: radiation-free technology; non-invasive lesion detection; X-ray free breast screening; MammoWave's dielectric breast response; supervised machine learning



Citation: Rana, S.P.; Dey, M.; Loretoni, R.; Duranti, M.; Ghavami, M.; Dudley, S.; Tiberi, G. Radiation-Free Microwave Technology for Breast Lesion Detection Using Supervised Machine Learning Model. *Tomography* **2023**, *9*, 105–129. <https://doi.org/10.3390/tomography9010010>

Academic Editor: Emilio Quaia

Received: 12 December 2022

Revised: 8 January 2023

Accepted: 9 January 2023

Published: 12 January 2023



Copyright: © 2023 by the authors. Licensee MDPI, Basel, Switzerland. This article is an open access article distributed under the terms and conditions of the Creative Commons Attribution (CC BY) license (<https://creativecommons.org/licenses/by/4.0/>).

1. Introduction

Breast cancer is the most common cancer in women worldwide, affecting 1 in every 8 women [1]. Mammography is the gold standard technology for breast screening but it has ionizing radiation which leads to potential harms for patients; specifically, the cumulative effect of routine mammography screening may increase women's risk of developing radiation-induced breast cancer [2]. Thus, age and screening frequency have been defined taking into account mammography risk-benefit ratio. Also, women feel some pain and discomfort [3] when undergoing mammography. Specifically, many women avoid mammography screening by fear of pain, embarrassment, discomfort, and radiation [1]. Additionally, the level of anxiety about the screening outcome is a tangible factor reducing mammography screening adherence, although the attitude differs depending on the age, profession, marital status, ethnicity, racial and educational differences [4,5].

To overcome the fear of pain, discomfort and ionizing radiation exposure issues, a novel device (i.e. MammoWave) based on low-power radio-frequency signals has been developed for breast lesion detection by UBT S.R.L. (Italy) team [6].

Moreover, in some cases, lesions prove difficult to detect from mammography, especially when the breast is highly dense [7–9], or if the breast comprises small, elongated salt-like microcalcification particles [10]. However, the evolution of machine learning (ML) algorithms and the greater availability of medical datasets from different modalities is enabling improved assisted detection and better performance hopes [11–13].

A recent case study on early breast cancer detection using AI methods from the mamographic images has been demonstrated in [14]. This study focus on the data collected from UK and US clinical trials. They shown a cancer case (small, irregular mass with associated microcalcifications and) that was missed by six readers in the examination, but correctly identified by the AI system. In this case three level deep learning was used to train the model for the breast cancer detection. In [15], a background on the key ethical, technical, legal and regulatory challenges of AI in breast imaging and performance in breast screening have been provided.

Recently, microwave-based techniques have emerged and received attention as an alternative breast-screening tool [6,16–19]. Ultrawide band microwave breast imaging (UWB-MWBI) demonstrates strong evidence of the dielectric property contrast between healthy and malignant tissues. Usually, a multistatic or monostatic radar mechanism is employed to measure the dielectric property contrast of breast tissues in the spectrum between 0.5 GHz to 9 GHz [20,21]. Hitherto, seven clinically tested MWBI operational systems have been reported in the literature such as; (a) UBT Srl, Italy who designed a MWBI system, named MammoWave, differentiate healthy tissues and tissues with lesions. MammoWave has been tested on 150 patients [22]; (b) Dartmouth College, USA, constructed a MWBI device for breast cancer identification where patterns were inspected by a the Surgical Pathology team at Dartmouth-Hitchcock Medical Center (DHMC). The trial was performed with 150 patients with and without lesions [23]; (c) Multistatic Array Processing for Radiowave Image Acquisition (MARIA) system was developed at the University of Bristol, UK and a clinical trial was carried with over 300 patients including healthy and lesion breast patterns [24,25]; (d) Tissue Sensing Adaptive Radar (TSAR) system was developed at the University of Calgary, CA and a clinical trial was reported with a small group of patients [26,27]; (e) Southern University of Science and Technology, China was constructed a MWBI imaging system and completed their first trial with a small group of patients [28]; (f) Hiroshima University, Japan trialled a MWBI for cancer identification with a small group of patients [29]. Additionally, McGill University, Canada [30] and Shizuoka University, Japan [31] have also developed their own MWBI system and recently started trials.

Microwave breast screening is non-ionising, non-invasive, and painless as it does not include any form of breast compression. A handful of microwave-based studies have been performed by researchers to detect breast cancer using real data, with the majority investigated using either numerical simulations or with phantoms. UBT Srl's MammoWave is one of the few Ultra-Wide Band (UWB) based microwave breast screening prototypes built, tested, and validated. MammoWave, uniquely functions in air with 2 antennas rotating in the azimuth plane, operating within the frequency band of 1–9 GHz. MammoWave examinations record the complex S_{21} (backscattered (returned) complex signals), in the frequency domain. Artefact removal is performed through appropriate mathematical procedures, namely rotation subtraction [32,33].

Contribution towards This Research

This work demonstrates that Machine learning (ML) can help understand phenomena from the frequency spectrum collected through MammoWave in response to the stimulus, segregating breasts with and without lesions. Specifically, ML can recognise the MammoWave signal response of breasts with no radiological finding (NF) and breasts with radiological findings (WF), i.e., with lesions (finding) which may be benign or malignant. Contributions of this study are: (a) the experiment has been performed across 61 breasts, enabling the exploration of lesions with different dimensions. (b) The new data appear

differently in the hyperplane, motivating the authors to explore Gaussian kernel of SVM alongside of quadratic kernel (SVM_Q) and Gaussian kernel (SVM_G), which are found to be more efficient in this case. (c) Making better use of the frequency response signals has been explored and experimentally it is shown that 50 components obtained using principal component analysis (PCA) provide best classification in this case. (d) The prediction results have been analysed by the team of researchers and radiologists through statistical measurements to understand the false positive and negative classifications, revealing that lesion size and breast density have effect on microwave response as well as ML predictions.

2. Materials and Methods

A diagrammatic interpretation of the proposed work is presented in Figure 1. Each breast has its own correspondent output of the radiologist study assessment, which has been used as gold standard for categorization of the breasts in two categories: breasts with no radiological finding (NF), and breasts with radiological findings (WF), i.e., with lesions which may be benign or malignant.

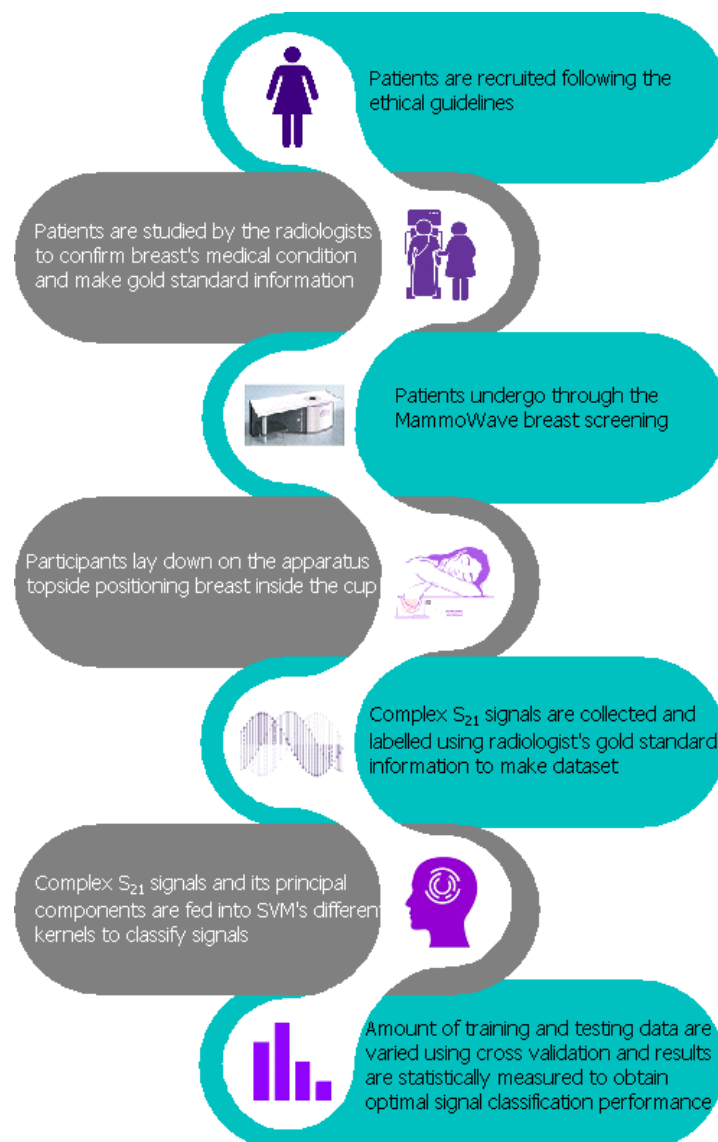


Figure 1. Proposed flow chart of MammoWave signal classification for the breast lesion detection.

Regarding the radiological study review, the radiologist assessment (NF/WF) used (accordingly to his/her opinion) one or more of the following conventional techniques:

mammography, performed using Selenia LORAD Mammography System (Hologic, Marlborough, MA, USA); echography, performed using the MyLab 70 xvg Ultrasound Scanner (Esaote, Genova, Italy); magnetic resonance imaging, performed through a 3.0 T MAGNETOM scanner (Siemens Healthcare, Erlangen, Germany). Gold standard labels of the breasts (NF or WF) have been employed to train and test the ML algorithms to automatically identify breast response signals backscattered from lesions via the MammoWave. The approach follows six primary steps: patient's undergo breast examinations through conventional approaches and breast type annotation (WF or NF) by the resident radiologist; subsequently, patient's undergo breast examination through MammoWave and the microwave signal data is collected. Once this is done, classification of resulting microwave signals is performed. The reduction of microwave feature space applying PCA to improve the classification result then follows. Finally, classification of signals employing only the real fragments of the complex signals, reduction of real part's feature space for improving the classification result. Each phase is explained in the following subsections.

The proposed research aims to identify the optimal classification settings for the research question using the components of complex S_{21} numbers. There are four possible ways to employ complex numbers (not alter the form of the original signal) and perform the classification task: (i) applying actual complex S_{21} responses, (ii) using features extracted from the complex S_{21} responses, (iii) using resistance values (real part of the complex S_{21} responses) from the transmitted voltage and current (reactance or imaginary part of S_{21} varies inversely with increasing frequency thus unsuitable for this classification task), (iv) using features extracted from the real part of S_{21} . The possible classification directions involved in the proposed study to improve breast lesion identification performances detailed in the later section.

- MammoWave breast signal classification considering features extracted from the complex S_{21} responses. Features have been extracted using PCA a powerful mathematical tool for multivariate data transformation. SVM_Q has been chosen for the ML task applying the team's previous research. Subsequently, SVM_G has been experimented alongside observing spherical data shapes for improved classification SVM_G performed better than SVM_Q here, thus SVM_G has been further adopted for the following classification tasks.
- MammoWave breast signal classification considering real parts of complex S_{21} responses and employing SVM_G .
- MammoWave breast signal classification considering features extracted (by PCA) from real parts of complex S_{21} and employing SVM_G .

Characteristics of the data used in each of these stages and their performance summaries are explained in the following sections.

Apparatus Description and Data Collection

The MammoWave device (shown in Figure 2a) has been designed by Umbria Bio-engineering Technologies (UBT), Italy. The device comprises a cylindrical aluminium container equipped with a chamber and cup to comfortably place the breast when women (or, participants) lay down to be screened. There is one transmitting (t_x) and one receiving antenna (r_x) which operate at 1 to 9 GHz frequency to obtain the breast's response to the applied microwave signals. The 2 antennas rotate around the breast, illuminating it from a number of angles. Figure 2b displays how patients undergo the MammoWave's breast examination, placing the breast inside the chamber with no breast compression required. To support all patients, three different cup sizes are available, and the best fit for the patient breast is selected. The largest cup has a diameter of 135 mm; thus, it cannot accommodate very large breasts. The cups have the following features. They are made using polylactic acid (PLA) to ensure biocompatibility [34] and with a width of 1 mm. This 1 mm thickness is based on modelling and experimental investigations by the team which demonstrated that this thickness has no effect on the microwave imaging outcomes [35].

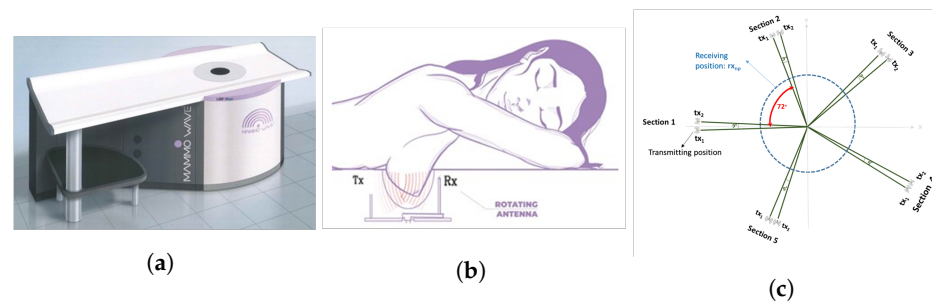


Figure 2. (a) MammoWave device designed by Umbria Bioengineering Technologies (UBT), Italy. (b) Patient's breast examination procedure with MammoWave. (c) Pictorial view of the transmitting-receiving antenna positions of MammoWave measurement.

The functioning principle of the MammoWave system is based on the dielectric properties (i.e., relative dielectric constant and conductivity) contrast between breast normal tissue and tissue with lesions at microwave frequencies. The antennas inside the container (covered to absorb microwaves) are fitted at the constant height, in free space and can rotate across the azimuth for collecting the microwave signals from diverse angular locations. The transmitting and receiving antennas are attached to a 2-port VNA (Cobalt C1209, Copper Mountain, Indianapolis, IN) that operates up to 9 GHz. Measurements have been accomplished by recording the complex S_{21} in a multi-bistatic fashion. For every transmitting and receiving spot, the complex S_{21} is gathered from 1 to 9 GHz, along with 5 MHz sampling. Let, r_x rotate across the azimuth collecting the microwave signals from diverse angular at a radius a_0 . The received signals can be expressed as, $n = 1, 2, \dots, 80$, denotes the receiving points; $m = 1, 2, \dots, 5$ indicates the transmitting sections, $p = 1, 2$ indicates the position inside each transmitting section; and f is the frequency.

MammoWave uniquely functions in air with 2 antennas rotating in the azimuth plane, operating within the frequency band of 1–9 GHz. The 2 antennas, one transmitting and one receiving, both rotate around the breast, illuminating it from a number of angles. MammoWave examinations are performed by recording the S_{21} (backscattered (returned) complex signals), in the frequency domain. Artefact removal is performed through appropriate mathematical procedures, namely rotation subtraction [32,33]. The MammoWave system has been employed to collect patient data: according to the conventional radiologist review, 25 breasts without lesions and 36 breasts with lesions, have been used in the work. Different S_{21} signatures are found when the microwave signals interact through breast tissues. This signature is due to the contrast in dielectric properties i.e., permittivity and conductivity, within the spectrum of microwave frequencies as they pass through the breasts. A high contrast (up to 5) has been reported [36] between healthy breast tissue and malignant tissue, while recent studies confirm a high contrast only between fatty and malignant breast tissues, while it decreases between healthy fibro glandular and malignant tissues [37].

MammoWave removes the need for applying any matching liquid. For each breast, measurements have been performed recording the complex S_{21} in a multibistatic fashion. Specifically, we employed here 15 transmitting positions, displaced in 5 triplets centred at 0° , 72° , 144° , 216° , and 288° ; in each triplet, the transmitting positions are displaced by 4.5° . For each transmitting position txm , the receiving antenna is moved to measure the received signal at 80 receiving points rxn , equally spaced along the azimuth of 4.5° . For each transmitting and receiving position, we recorded the complex S_{21} in the frequency band from 1 to 9 GHz, using a frequency sampling of 5 MHz. Thus, that for each breast, the raw-data can be represented by a matrix of complex S_{21} with dimension $(15 \times 80) \times (1601 \times 2)$. Figure 2c shows a pictorial view of the measurements setup. A breast scan is completed in ~ 10 min, whilst the person is in a horizontal face down position on a thin mattress, with no breast compression. Numbers and displacements of transmitting and/or receiving positions can be changed [35]; specifically, an increase of the number of transmitting and/or receiving positions will lead to an increase of the measurement time. We verified

in phantoms that the proposed configuration allows detection in a reasonable measurement time [35], i.e., ~ 10 min, a duration which is similar to a traditional X-ray breast screening examination.

The MammoWave feasibility clinical validation has been performed in Perugia and Foligno Hospitals, Italy (Ethical Committee of Umbria, Italy, approval N. 6845/15/AV/DM of 14/10/2015, N. 10352/17/NCAV of 16/03/2017, N 13203/18/NCAV of 17/04/2018). The correspondent clinical protocol aims to quantify the device's accuracy in breast lesions detection. As an inclusion criterion, the subjects should have a radiologist study output obtained through conventional examinations (mammography and/or ultrasound and/or magnetic resonance imaging) within the last month. The protocol and procedures were in accordance with institutional and ethical standards in research, with Declaration of Helsinki (1964) and its later amendments.

For this study, we used data of 61 breasts, each one with its own correspondent radiologist study review output, which has been used as gold standard for classifying the breasts in two categories: breasts with no radiological finding (NF), and breasts with radiological findings (WF), i.e., with lesions which may be benign or malignant. Some details of the detected or suspected lesions have been collected for WF breasts; moreover, pathology and/or clinical follow-up has been performed for lesions' final assessment (benign/malignant). The subject's information is charted in Table 1. In Table 2 some details of the radiologist study review are given for WF breasts.

Table 1. Summary of the patient population used in this study.

Name of Parameters	Values
Total patients	34
Total subjects (breasts)	61
Number of patients age between 20–49 year	23
Number of patients age between 50–80 year	38
Mean of patient's age (in year)	52
Standard deviation of patient's age (in year)	12

Table 2. Details and related radiologist's review for the breasts with radiological findings (WF).

Age	Breast (L/R)	ACR Breast Density	Mammography BI-RADS	Echography BI-RADS	Radiologist's Output Details: Sizes (mm) & Notes (if Available)	Pathology or 1-Year Clinical Follow-up Output
48	L	D	3	-	Microcalcifications	Benign
65	L	C	4	-	Cluster of microcalcifications	Benign
40	L	B	2	2	Three masses: 15 mm, 21 mm, and 23 mm	Benign
	R	B	2	2	Microcalcifications	Not available
52	L	C	5	-	Microcalcifications	Malignant
47	L	D	2	2	Microcalcifications	Benign

Table 2. Cont.

Age	Breast (L/R)	ACR Breast Density	Mammography BI-RADS	Echography BI-RADS	Radiologist's Output Details: Sizes (mm) & Notes (if Available)	Pathology or 1-Year Clinical Follow-up Output
55	R	C	2	2	1.6 mm microcalcifications	Benign
	L	C	2	2	3.8 mm microcalcifications	Benign
51	L	C	2	2	Presence of metallic marker	Benign
54	R	A	2	2	Microcalcifications	Benign
77	R	D	-	5	17 mm mass	Malignant
61	R	C	4	-	Multifocal lobular type suspected carcinoma (MRI BI-RADS 4)	Malignant
	L	C	2	-	Macrocalcification and Focal contrast enh. (MRI BI-RADS 3)	Not available
50	L	B	2	2	10 mm mass	Benign
67	L	C	4	-	Microcalcifications	Malignant
49	L	A	3	-	Microcalcifications	Benign
70	L	D	3	4	Mass	Malignant
42	L	C	2	3	7 mm mass, hypoechoic	Benign
67	L	B	3	-	Architectural distortion	Benign
56	R	B	4	4	31 mm mass, hypoechoic, irregular borders	Malignant
43	R	D	1	3	12 mm mass	Benign
51	L	C	3	-	Microcalcifications	Benign
59	L	B	-	4	11 mm areolar, suspicious of malignancy	Malignant
40	L	D	2	2	30 mm mass	Benign
35	R	C	2	3	7 mm, hypoechoic	Benign
37	L	A	2	3	25 mm mass	Benign
43	R	B	3	2	Microcalcifications	Malignant
54	R	B	2	2	18 mm mass	Benign
49	L	A	2	3	16 mm mass	Benign
56	L	D	4	4	27 mm mass	Malignant
63	L	A	3	4	6 mm mass	Malignant
55	R	C	4	4	23 mm mass	Malignant
	L	C	2	2	Multiple cysts	Benign
64	R	B	3	-	1.6 mm microcalcifications	Benign
37	R	-	-	3	15.4 mm mass	Benign
	L	-	-	2	Multiple cysts	Not available

3. Proposed Methodology

The proposed ML for segregating breasts with and without lesions from the MammoWave signal consist of mainly three stages. At first the PCA has been applied to the collected data from 61 breasts for the optimum use of the frequency response signals. Then SVM was applied on the extracted feature by PCA for the classification and results were compared with two different kernel functions. Finally, the performance of the classification method were analysed and results were validated statistically. A flow chart of the proposed method shown in Figure 3.

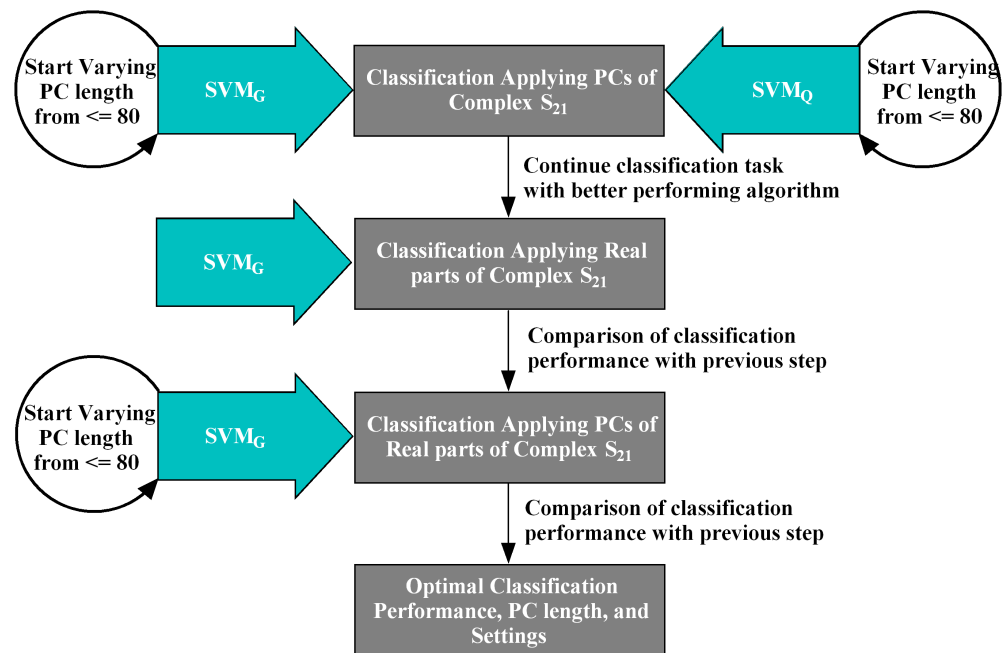


Figure 3. A Flowchart of the classification stages involved in the proposed ML experiment. SVM_G and SVM_Q have been trialed and compared, employing PCs of the complex S_{21} data (raw data). The investigation continued with SVM_G , comparing its performance with SVM_Q . Subsequently, real parts and PCs obtained from the real parts of the complex S_{21} have been employed in the second and third stages respectively to classify the NF-WF signals by SVM_G . The optimal performance attained in the third stage applying PCs of real parts of complex S_{21} with SVM_G .

3.1. Principal Component Analysis

Principal components (PCs) have been extracted from the MammoWave's complex S_{21} responses, represented as $\lambda = \sum_{n=1}^{NF=1601} \lambda_{real}(n) + j\lambda_{img}(n)$, where n is the number of frequencies, λ_{real} and λ_{img} are the real and imaginary components respectively. The λ_{real} indicates the resistance of the dielectric materials (tissues) to the transmitted signals with n number of frequencies. The λ_{img} indicates the capacitance of the dielectric materials (tissues) of the transmitted signals with n number of frequencies. PCA has been implemented on both λ_{real} and λ_{img} components to extract principal components (PCs) for classifying signals obtained from breast considering covariance matrix and Eigen vector.

3.2. Basic Theory of the Proposed Algorithms

Several ML algorithms present for classification in the literature, although the selection of appropriate methods is quite intuitive and needs to be determined heuristically. In support vector machine (SVM), each breast signal data consist of S -dimensional feature vector and a class is refer to each corresponding pattern [38]. SVM assigns a class label to each signal data pattern on the basis of its position with respect to a decision hyperplane, which defines by Equation (1), where, b is bias and x is variable. The distance between those boundaries of a margin area around the decision hyperplane, is called the margin width defined by $w^T x + b = \pm 1$. In SVM, kernel function must be chosen in order to achieve better performance. It defines the structure of the high-dimensional feature space to determine maximise margin hyperplane Equation (2).

$$w^T x + b = 0 \quad (1)$$

$$\hat{w}, \hat{b} = \arg \min_{w,b} \left(\frac{1}{2} \|w\|^2 \right) \quad (2)$$

The experimented data distribution appears non-linearly separable and to avoid model overfitting, hence the quadratic kernel (SVM_Q) and Gaussian kernel (SVM_G) function have been chosen for this NF and WF signal classification.

SVM_Q have been employed to differentiate data points by minimising the gap between the two groups. The considered quadratic function is obtained by the optimisation problem define by Equation (3), where, x_i, x_j are real valued vectors, d is degree of polynomials, here $d = 2$ (quadratic), since larger value tend to overfit.

$$k(x_i, x_j) = (x_i \cdot x_j + 1)^d \quad (3)$$

SVM_G is popular kernel function for its excellent learning performance which can approximate bounded and continuous functions arbitrarily well, defined by Equation (4). The non-linear Euclidean distance controlled by kernel width parameter σ , which has great influence for the classification accuracy. It determine the feature space that the samples will be mapped onto. As $\sigma \rightarrow 0$, where all samples is classified correctly, but learning generalisation performance is poor and SVM can not classify new samples; whereas $\sigma \rightarrow \infty$, the whole sample is classified as one class. This function creates the best hyperplane to classify the subjects here.

$$k(x_i, x_j) = \exp\left(-\frac{\|x_i - x_j\|^2}{2\sigma^2}\right), \quad (4)$$

3.3. Performance Analysis

In this work, 61 breasts were used, of which: 26 NF and 35 WF breasts (see Table 2). A summary statistic of two raw microwave scan population is shown in Table 3. Quantitative range of features of each population are not significantly high and compact in nature. Hence, application of normalisation could make the features insignificant for machine learning application and has been avoided in this work.

Table 3. Approximated quantitative summary of raw S_{21} signals, as these values may vary with the addition of new patients.

Breast Type	Mean	Maximum	Minimum	Median	Standard Deviation	Variance
No-Finding (NF)	2.179×10^{-5}	0.114	-0.105	-8.286×10^{-5}	0.011	4.578×10^{-7}
With-Finding (WF)	1.985×10^{-5}	0.118	-0.108	-1.640×10^{-4}	0.011	4.651×10^{-7}

MammoWave's breast screening data is non-linearly separable and logistic regression assumes the linearity between dependent and independent variables. Hence, logistic regression algorithm has not been attempted for classifying the data into WF and NF classes. In case of decision tree, a small change in the test/unseen data can cause a large change in the structure of the decision tree causing instability. Also, decision tree is very much sensitive to the new data which may put the whole system into risk. Therefore, decision tree has not been employed for the classification task. The leading supervised and non-linear classifiers such as, k-nearest neighbour, and multi-layer perceptron neural network, support vector machines have been attempted before and reported in the previously published article [39]. Support vector machine's quadratic (SVM_Q) kernel has been selected following the previous research findings. As SVM_Q was applied on a limited number of patients after performing dedicated S_{21} pre-processing for artefact removal. Here, with the aim of exploring the applicability of ML algorithms directly to S_{21} , i.e., raw-data and observing spherical data shapes. Hence, the two algorithms SVM_G and SVM_Q are investigated and compared for obtaining improved classification performance. Also, the proposed work explores the possible way for improving previous results using principal component analysis (PCA) [40] on raw S_{21} signals (described in Section 4.1), real parts

of S_{21} signals (described in Section 4.2, and PCA over real parts of S_{21} signals (described in Section 4.3) minimising false positive-negative signals and identify the appropriate numerical sequence for the classification of NF and WF signals. It is possible that even the data are labelled into two groups by the radiologists but the finite differences are not suitable for classification when the elements of S_{21} and principal components are prepared. Therefore, two sample t -test has been implemented three times before applying machine learning algorithm. Null hypothesis (H_0) of the proposed work assumes the S_{21} values or extracted features applying PCA of two population (NF and WF group) comes from independent random samples from normal distributions with equal means and equal but unknown variances. However, the alternative hypothesis (H_a) assumes the S_{21} values or extracted features applying PCA of two population (NF and WF group) comes from unequal means. Hence, H_a needs to be accepted in order to perform NF-WF signal classification. The ideal importance level $\alpha = 0.05$ has been expected for tolerating and dismissing the null hypothesis, where p -value has been thought about for choosing the factual importance. Additionally, the confidence interval for the distinction in populace method for NF and WF signals have been considered, where C_L and C_U show the lower and upper limits of the certainty span. The ML experiment has been divided into two major parts; (a) realisation of optimal feature combination through training and validation phase (described in Sections 4.1–4.3), (b) testing the trained model with optimal settings (described in Section 4.4). The data have partitioned using Monte Carlo cross validation (MCCV) [41] in both cases. This is done because it randomly partitions to select the training and validation dataset helping to understand the impact of risk and uncertainty in NF-WF breast signal prediction. The performance outcomes (statistical metrics) have been aggregated and averaged over all the rounds. A number of statistical metrics, accuracy, sensitivity, and specificity have been used to investigate the classification performance of the classifiers [42]. Subsequently, Matthews Correlation Coefficient (MCC) [43] has been implemented to investigate the classification outcomes and estimate quality of classification and probability of the informed decision respectively. Receiver operating characteristic (ROC) curve has been generated for the optimally performing ML model to explain the diagnostic competence and steadiness of the classification system with different discrimination threshold. The hyperparameter optimisation has been conducted in training-validation phase and best operating point decided analysing ROC curve. While the optimised parameters and ROC threshold have been used to produce final testing result (described in Section 4.4).

4. Results Analysis

According to the radiologist's review, a total of 34 patients have been included in this study, with a total of 61 breasts examined (see Table 1). Among the total examined breasts, 25 NF and 36 WF breasts underwent the MammoWave exam, collecting S_{21} raw data. WF breasts are breasts having lesions, which may be benign or malignant; lesions were found to have dimensions ranging up to 32 mm. The raw-data of each breast are represented by a matrix of complex S_{21} having dimensions 1200×3202 (described in Section 2), where each complex signal contains 1601 real and 1601 imaginary components. Hence the classification experiment has been conducted on total 73,200 signals (31,200 NF signals and 42,000 WF signals). Complex S_{21} raw data signals and its components have been individually employed for experimental purpose, where prediction efficiency is influenced by the discriminating ability of individual features i.e., real, and imaginary parts of complex S_{21} . Each simulation has been run twenty-five times to observe the result stability before reporting average performance metrics.

4.1. Classification Applying PCs of Complex S_{21}

Figure 4 shows the percentage of total variance obtained from each PC for two different breast S_{21} 's, and the first 80 PCs are found to be quantitatively significant. This is because numerically, the variance values are a factor of 10^{-5} after the 80 PCs, hence extremely

small and quantitatively insignificant, thus the team will investigate the first 80 PCs only. Figure 4a,b show an example of percentage variance for the first 80 PCs, where the x -axis and y -axis represent the number of components and percentage of variance respectively. Figure 4a displays the percentage of variance of a NF breast and Figure 4b describes the percentage of variance of a WF breast. Hence, the experiment for reduced feature space has been started from 80 PCs and features are continually eliminated until the optimal performance achieved with this feature setting. Maximum variances of 23.774% and 32.289% were achieved for NF and WF breast contained the within 80 PCs mentioned above.

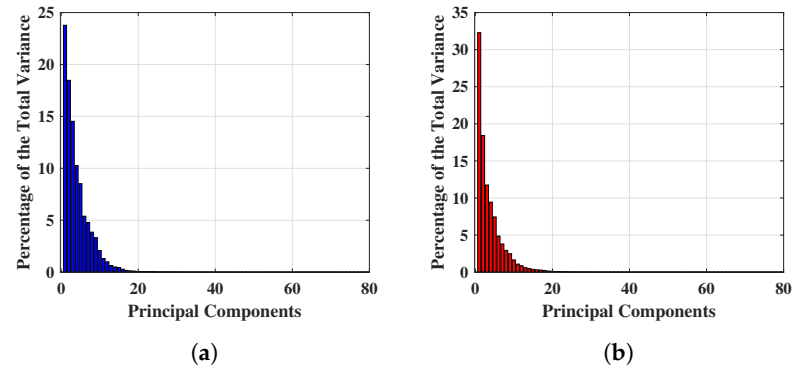


Figure 4. Example of significant variance achieved applying PCA on complex S_{21} signals. (a) Significant variance achieved applying PCA on complex S_{21} signals of a NF breast. (b) Significant variance achieved applying PCA on complex S_{21} signals of a WF breast.

Table 4 shows the outcomes of the t -test, where $p < \alpha$ rejects the null hypothesis H_0 ($H_0 = 1$), accepts alternative hypothesis H_a , and the true mean of the population belong between -3×10^{-5} to -1.500×10^{-5} . Hence, the acceptance of alternative hypothesis indicates that the λ_{real} data comes from populations with unequal means and can be employed for NF-WF signal classification task.

Table 4. Two-sample t -test on PCA features extracted from MammoWave’s complex S_{21} data.

Null Hypothesis (H_{null})	Probability (p)	Confidence Interval (C_L)	Confidence Interval (C_U)
1	7.516×10^{-10}	-3.000×10^{-5}	-1.500×10^{-5}

The results obtained here are from the selection of 80 PCs based on the investigation of Figure 4. With the PC length varied from 80 to 40 at 10-unit intervals, the variation of the classification performance of SVM_Q and SVM_G was obtained and tabulated in Table 5. Accuracy (A_c), sensitivity (S_e), specificity (S_p), and the Matthews Correlation Coefficient (MCC) performance measure have been computed to investigate the predictions provided by SVM_Q and SVM_G . Table 5a,b show the classification performance of SVM_Q and SVM_G respectively. Each set of performance metrics varying principal components (PCs) have been included here. The optimal performance of both SVM_Q and SVM_G in this case was obtained in the first 50 PCs. Outcomes have been plotted in Figure 5 for comparing the performance in graph. Figure 5a,c,e,g show the A_c , S_e , S_p , and MCC respectively obtained from classification applying SVM_Q . The best sensitivity S_e of 0.448 obtained by SVM_Q employing 50 PCs which is not significant and satisfactory for breast lesion identification. Though, achieved the specificity S_p is 0.820 but the misclassification of breast WF signals (signals reflected from lesions) i.e., false positives lowered the overall A_c and MCC . The best set of performance of SVM_Q achieved employing 80% of training data (and 20% validation data) with 50 PCs, where $A_c = 66.80\%$, $S_e = 44.80\%$, $S_p = 82\%$, and $MCC = 29\%$.

Table 5. The classification results over reduced feature space (i.e., extracted features from MammoWave’s original frequency response) after applying SVMs. (a) The classification results over reduced feature space (i.e., extracted features from MammoWave’s original frequency response) after applying SVM_Q. (b) The classification results over reduced feature space (i.e., extracted features from MammoWave’s original frequency response) after applying SVM_G.

Feature Dimension →	PC-80				PC-70				PC-60				PC-50				PC-40			
Validation Data ↓	A_c	S_e	S_p	MCC																
95%	0.644	0.509	0.737	0.251	0.635	0.434	0.774	0.221	0.626	0.489	0.720	0.213	0.616	0.416	0.754	0.180	0.601	0.410	0.733	0.150
90%	0.670	0.510	0.781	0.302	0.653	0.471	0.781	0.264	0.647	0.468	0.772	0.251	0.630	0.422	0.775	0.210	0.611	0.368	0.779	0.161
85%	0.682	0.518	0.797	0.328	0.670	0.501	0.787	0.301	0.654	0.455	0.793	0.264	0.642	0.427	0.791	0.235	0.621	0.370	0.796	0.183
80%	0.690	0.522	0.807	0.345	0.680	0.535	0.781	0.326	0.666	0.458	0.811	0.289	0.649	0.423	0.806	0.248	0.629	0.391	0.794	0.202
75%	0.693	0.528	0.808	0.352	0.684	0.516	0.799	0.330	0.666	0.462	0.808	0.289	0.653	0.430	0.808	0.257	0.632	0.343	0.832	0.201
70%	0.706	0.565	0.804	0.380	0.689	0.542	0.791	0.345	0.676	0.498	0.799	0.313	0.658	0.434	0.813	0.268	0.630	0.345	0.830	0.201
65%	0.704	0.549	0.812	0.376	0.695	0.551	0.795	0.357	0.673	0.488	0.801	0.305	0.654	0.433	0.807	0.259	0.630	0.318	0.847	0.195
60%	0.708	0.570	0.805	0.387	0.692	0.527	0.808	0.350	0.676	0.487	0.808	0.313	0.659	0.443	0.808	0.270	0.634	0.349	0.832	0.207
55%	0.715	0.559	0.824	0.400	0.700	0.531	0.818	0.366	0.681	0.492	0.813	0.324	0.662	0.425	0.826	0.277	0.629	0.301	0.855	0.189
50%	0.717	0.583	0.809	0.405	0.702	0.536	0.818	0.371	0.682	0.501	0.809	0.327	0.663	0.423	0.831	0.280	0.629	0.319	0.846	0.195
45%	0.718	0.577	0.815	0.405	0.697	0.541	0.805	0.360	0.683	0.503	0.807	0.327	0.661	0.417	0.829	0.273	0.634	0.328	0.848	0.207
40%	0.713	0.568	0.813	0.394	0.701	0.532	0.819	0.368	0.680	0.494	0.808	0.320	0.661	0.424	0.825	0.273	0.636	0.345	0.838	0.211
35%	0.718	0.571	0.820	0.406	0.708	0.558	0.811	0.384	0.685	0.501	0.812	0.331	0.666	0.440	0.822	0.286	0.637	0.356	0.830	0.213
30%	0.718	0.570	0.822	0.407	0.714	0.564	0.818	0.396	0.686	0.499	0.817	0.335	0.665	0.428	0.830	0.284	0.631	0.307	0.857	0.197
25%	0.722	0.576	0.822	0.413	0.706	0.559	0.806	0.379	0.690	0.503	0.818	0.341	0.668	0.423	0.839	0.291	0.637	0.324	0.857	0.216
20%	0.723	0.583	0.818	0.415	0.710	0.565	0.810	0.388	0.688	0.513	0.807	0.336	0.668	0.448	0.820	0.290	0.638	0.327	0.855	0.217

Table 5. Cont.

Feature Dimension →	PC-80				PC-70				PC-60				PC-50				PC-40			
Validation Data ↓	A_c	S_e	S_p	MCC																
95%	0.633	0.118	0.990	0.233	0.633	0.129	0.983	0.228	0.641	0.163	0.972	0.242	0.649	0.235	0.936	0.247	0.649	0.311	0.883	0.241
90%	0.664	0.202	0.985	0.320	0.674	0.237	0.978	0.338	0.677	0.264	0.964	0.334	0.687	0.350	0.923	0.342	0.682	0.381	0.890	0.322
85%	0.703	0.307	0.978	0.405	0.711	0.347	0.965	0.414	0.719	0.375	0.957	0.426	0.726	0.450	0.918	0.428	0.716	0.481	0.878	0.399
80%	0.731	0.383	0.972	0.461	0.736	0.414	0.960	0.467	0.748	0.456	0.950	0.485	0.756	0.532	0.912	0.491	0.736	0.538	0.874	0.445
75%	0.753	0.442	0.970	0.508	0.766	0.491	0.957	0.527	0.771	0.514	0.951	0.536	0.775	0.556	0.929	0.536	0.759	0.579	0.884	0.495
70%	0.779	0.501	0.972	0.559	0.792	0.548	0.960	0.579	0.793	0.566	0.951	0.579	0.794	0.612	0.921	0.573	0.778	0.619	0.888	0.534
65%	0.800	0.556	0.970	0.602	0.807	0.588	0.958	0.608	0.810	0.610	0.949	0.612	0.812	0.651	0.925	0.611	0.797	0.657	0.894	0.576
60%	0.815	0.595	0.969	0.631	0.826	0.630	0.962	0.648	0.827	0.651	0.950	0.647	0.828	0.690	0.923	0.642	0.809	0.682	0.897	0.600
55%	0.832	0.631	0.972	0.664	0.842	0.670	0.960	0.678	0.842	0.680	0.955	0.678	0.842	0.710	0.935	0.674	0.820	0.699	0.904	0.625
50%	0.843	0.660	0.971	0.685	0.851	0.692	0.960	0.695	0.852	0.704	0.955	0.698	0.855	0.743	0.932	0.699	0.833	0.728	0.906	0.653
45%	0.857	0.690	0.973	0.712	0.866	0.715	0.971	0.729	0.866	0.734	0.957	0.726	0.870	0.763	0.943	0.731	0.844	0.743	0.914	0.675
40%	0.867	0.716	0.971	0.730	0.876	0.743	0.968	0.748	0.877	0.759	0.958	0.747	0.879	0.783	0.945	0.749	0.850	0.761	0.911	0.687
35%	0.881	0.740	0.978	0.760	0.887	0.764	0.974	0.772	0.885	0.773	0.964	0.765	0.883	0.795	0.944	0.758	0.861	0.772	0.924	0.713
30%	0.887	0.756	0.979	0.772	0.892	0.775	0.974	0.781	0.892	0.787	0.965	0.779	0.893	0.812	0.949	0.778	0.871	0.786	0.930	0.733
25%	0.891	0.763	0.981	0.781	0.906	0.804	0.975	0.807	0.897	0.795	0.969	0.790	0.900	0.825	0.951	0.792	0.873	0.799	0.924	0.736
20%	0.905	0.796	0.979	0.806	0.911	0.820	0.974	0.818	0.910	0.826	0.968	0.815	0.909	0.843	0.953	0.810	0.883	0.806	0.936	0.757

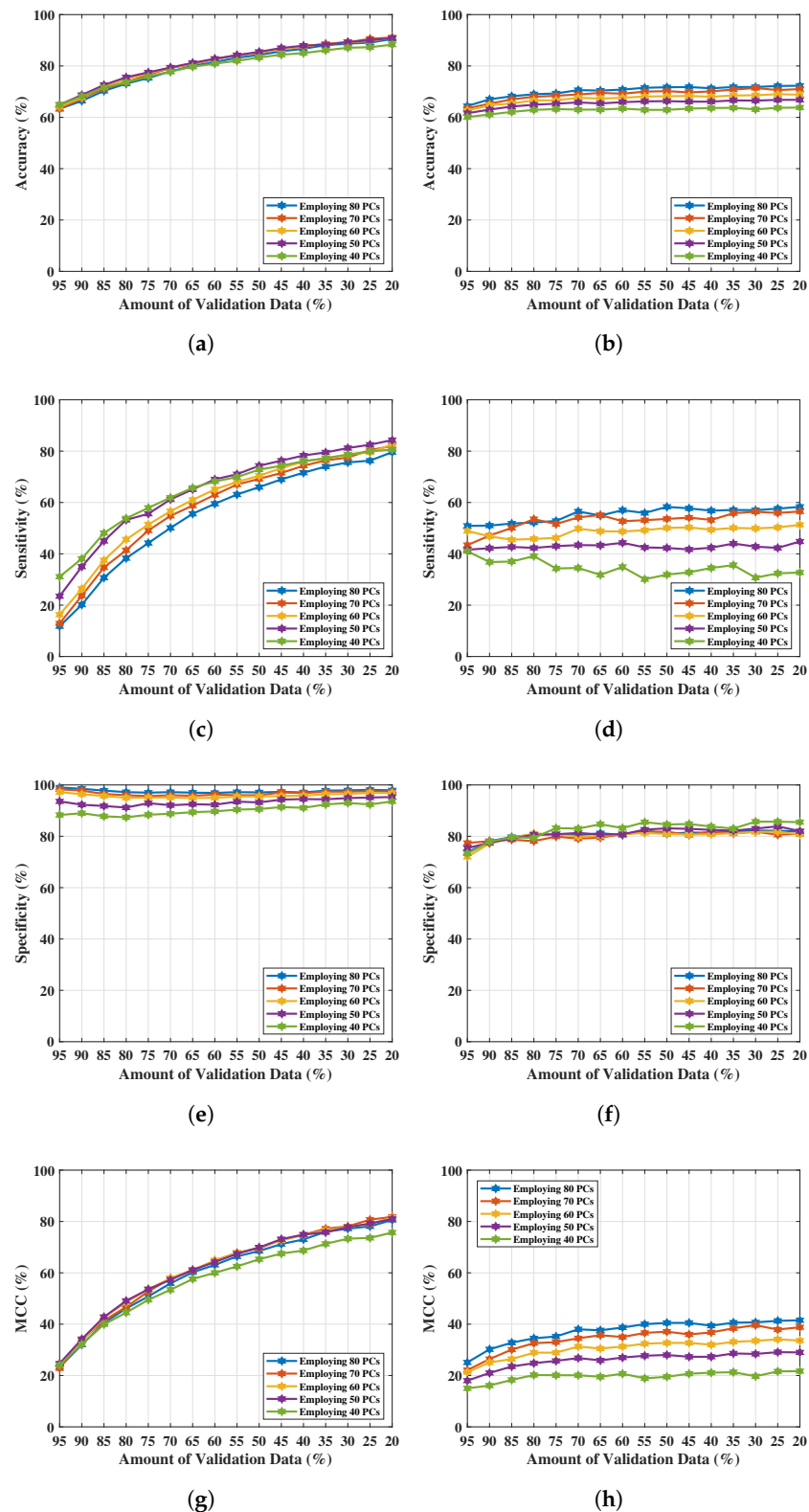


Figure 5. NF and WF signal classification results obtained from SVM_Q and SVM_G applying PCA over MammoWave’s complex S_{21} data. (a) Accuracy obtained from SVM_G varying PCs and validation data. (b) Accuracy obtained from SVM_Q varying PCs and validation data. (c) Sensitivity obtained from SVM_G varying PCs and validation data. (d) Sensitivity obtained from SVM_Q varying PCs and validation data. (e) Specificity obtained from SVM_G varying PCs and validation data. (f) Specificity obtained from SVM_Q varying PCs and validation data. (g) MCC obtained from SVM_G varying PCs and validation data. (h) MCC obtained from SVM_Q varying PCs and validation data.

Figure 5b,d,f,h exhibit A_c , S_e , S_p , and MCC respectively by implementing SVM_G . In case of SVM_G , all the achieved performance metrics are satisfactory. The best performance of SVM_G obtained using 80% of training data (i.e., 20% of validation data) with 50 number of PCs, obtained $A_c = 90.90\%$, $S_e = 84.30\%$, $S_p = 95.30\%$, and $MCC = 81\%$. Further reduction of PCs length (40 PCs) drops the performance of classification using SVM_G (shown in Figure 5 and Table 5b).

4.2. Classification Applying Real parts of Complex S_{21}

During the previously executed experiments SVM performed well with the Gaussian kernel, thus the SVM_G has been considered here to obtain optimal outcomes for NF and WF breast signal classification. Only real components $\sum_{n=1}^{NF} \lambda_{real}(n)$ from the complex S_{21} signals $\lambda_n = \sum_{n=1}^{NF=1601} \lambda_{real}(n) + j\lambda_{img}(n)$, $NF = 1601$, have been chosen for this classification employing SVM_G and the work flow stated in Figure 3. The resistance components $\lambda_{real}(n)$ have employed as features to inspect whether these are more revealing features for NF-WF signal prediction along with the SVM_G and increasing true predications.

$\lambda_{real}(n)$ data has been analysed and studied through two sample t -test for comparing the average values of $\lambda_{real}(n)$ from two different classes i.e., NF and WF signal data. Table 6 shows the outcomes of the t -test, where $p < \alpha$ rejects the null hypothesis H_0 ($H_0 = 1$), accepts alternative hypothesis H_a , and the true mean of the population belong between -6.600×10^{-5} to -4.600×10^{-5} . Hence, the acceptance of alternative hypothesis indicates that the $Real_{S_{21}}$ data comes from populations with unequal means and can be employed for NF-WF signal classification task.

Table 6. Two-sample t -test on real-parts of MammoWave's S_{21} data.

Null Hypothesis (H_0)	Probabilty(p)	Confidence Interval (C_L)	Confidence Interval (C_U)
1	8.864×10^{-27}	-6.600×10^{-5}	-4.600×10^{-5}

Table 7 shows the NF-WF signal classification performance using $\lambda_{real}(n)$ applying SVM_G . The best classification performance of SVM_G was obtained with 80% training data (i.e., 20% of validation data). Achieved metrics A_c , S_e , S_p , and MCC are 0.798, 0.704, 0.863, and 0.577 respectively. The performance metrics did not improve on the previous test (using PCs obtained from the actual complex S_{21} sequences). Sensitivity $S_e = 0.704$ clearly indicates the increment of false positive predictions or misidentification of WF (or, lesion) signals. These misidentifications affect the MCC measure ($= 0.577$) in the other way. All these results have been pictured in Figure 6. This parameter setting becomes unreliable as a significant number of misidentifications were found, also reflected in the performance metrics. The 20% validation data indicates 14,640 number of signals out of which approximately 3597 signals misidentified (false positive signals 2962 approx. and false negative signals 635 approx.) in each run.

Table 7. NF and WF signal classification results obtained from SVM_G applying real-parts of MammoWave's complex S_{21} data.

Validation Data	A_c	S_e	S_p	MCC
95%	0.623	0.400	0.777	0.190
90%	0.652	0.427	0.808	0.255
85%	0.673	0.455	0.824	0.303
80%	0.694	0.513	0.820	0.353

Table 7. Cont.

Validation Data	A_c	S_e	S_p	MCC
75%	0.709	0.542	0.825	0.385
70%	0.724	0.568	0.832	0.418
65%	0.729	0.578	0.834	0.430
60%	0.746	0.610	0.840	0.465
55%	0.751	0.615	0.847	0.478
50%	0.760	0.625	0.855	0.497
45%	0.767	0.640	0.855	0.511
40%	0.775	0.659	0.855	0.528
35%	0.779	0.660	0.862	0.538
30%	0.786	0.678	0.861	0.552
25%	0.793	0.685	0.868	0.567
20%	0.798	0.704	0.863	0.577

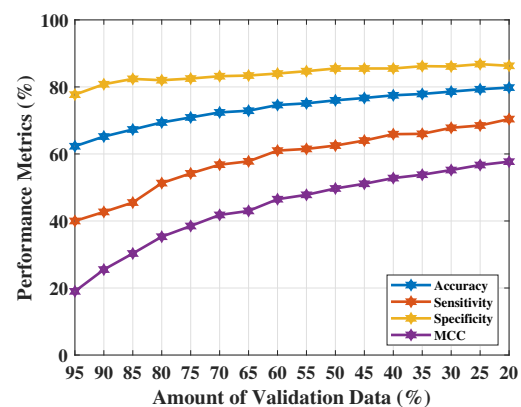


Figure 6. NF and WF signal prediction results (accuracy, sensitivity, specificity, and MCC) obtained using real parts of MammoWave's complex S_{21} signals applying SVM_G over different amount of validation data.

4.3. Classification Applying PCs of Real Parts of Complex S_{21}

The third phase of the proposed work has been performed by extracting principal components from $\lambda_{real}(n)$ and applying SVM_G for NF-WF classification (as stated in Figure 3). PCs extracted from $\lambda_{real}(n)$ are denoted as $\sigma_1, \sigma_2, \dots, \sigma_n$. Two vectors of variances (applying PC) have been selected from NF-WF breasts to study the magnitude of variances which has been employed to choose the number of PCs for classification task, as shown in Figure 7. Significant variance has been found upto 80 PCs ($\sigma_1, \sigma_2, \dots, \sigma_{80}$) and selected for NF-WF signal classification. Number of PCs have been varied anticipating an improved performance. In addition, the spherical data distribution and more compactness than before may help in better classification.

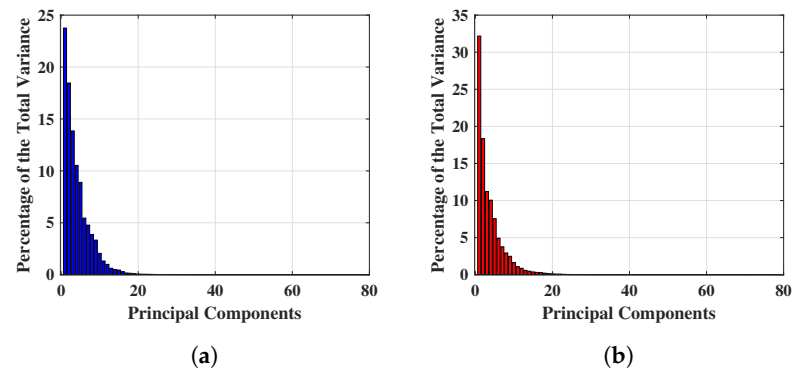


Figure 7. Example of significant variance achieved applying PCA on real part of complex S_{21} signals. (a) Significant variance achieved applying PCA on real part of complex S_{21} signals of a NF breast. (b) Significant variance achieved applying PCA on real part of complex S_{21} signals of a WF breast.

The variance of PCs are close to each other in Figure 7. Two sample t-test has been repeated on PCs to understand the capability to represent two signal groups and the data compactness. The probability has been found to be less than the significance level, $P < \alpha$. Hence, the t-test accepts alternative hypothesis H_a and clearly demonstrates the presence of two different means for two different populations. Subsequently, the difference between lower and upper boundary (-1.770×10^{-4} and -1.570×10^{-4}) is reduced which implies improved data compactness than before detailed in Table 8.

Table 8. Two-sample t-test on PCA features extracted from real-parts of MammoWave's S_{21} data.

Null Hypothesis (H_0)	Probabilty (p)	Confidence Interval (C_L)	Confidence Interval (C_U)
1	8.219×10^{-23}	-1.770×10^{-4}	-1.570×10^{-4}

Table 9. Classification results applying PCs extracted from real parts of MammoWave’s complex S_{21} signals with SVM_G .

Feature Dimension →	PC-80				PC-70				PC-60				PC-50				PC-40			
Validation Data ↓	A_c	S_e	S_p	MCC																
95%	0.632	0.118	0.990	0.232	0.632	0.127	0.983	0.224	0.638	0.150	0.977	0.237	0.650	0.243	0.932	0.248	0.652	0.313	0.887	0.248
90%	0.664	0.203	0.985	0.320	0.682	0.269	0.967	0.346	0.686	0.288	0.962	0.354	0.691	0.357	0.923	0.351	0.686	0.424	0.867	0.330
85%	0.704	0.308	0.979	0.407	0.712	0.351	0.964	0.416	0.712	0.362	0.957	0.413	0.729	0.464	0.913	0.433	0.711	0.482	0.870	0.388
80%	0.732	0.385	0.972	0.463	0.746	0.449	0.952	0.482	0.750	0.473	0.942	0.487	0.754	0.528	0.911	0.487	0.732	0.512	0.886	0.437
75%	0.754	0.442	0.971	0.509	0.767	0.494	0.957	0.529	0.766	0.503	0.950	0.524	0.777	0.580	0.915	0.538	0.758	0.579	0.883	0.493
70%	0.780	0.503	0.972	0.561	0.790	0.550	0.957	0.575	0.788	0.557	0.950	0.570	0.798	0.621	0.922	0.582	0.780	0.630	0.883	0.538
65%	0.800	0.555	0.971	0.602	0.812	0.605	0.955	0.617	0.810	0.601	0.956	0.615	0.814	0.658	0.922	0.614	0.792	0.649	0.891	0.565
60%	0.816	0.597	0.969	0.631	0.825	0.632	0.959	0.645	0.832	0.657	0.953	0.657	0.831	0.698	0.923	0.649	0.806	0.679	0.893	0.594
55%	0.833	0.633	0.973	0.667	0.842	0.672	0.958	0.677	0.844	0.681	0.956	0.681	0.846	0.718	0.935	0.682	0.822	0.702	0.905	0.628
50%	0.843	0.660	0.972	0.686	0.854	0.696	0.964	0.705	0.851	0.697	0.957	0.695	0.852	0.739	0.930	0.693	0.829	0.724	0.902	0.644
45%	0.858	0.690	0.973	0.713	0.864	0.714	0.968	0.724	0.866	0.727	0.963	0.727	0.865	0.765	0.935	0.721	0.841	0.731	0.918	0.670
40%	0.867	0.717	0.971	0.731	0.873	0.739	0.966	0.741	0.873	0.753	0.956	0.739	0.875	0.785	0.937	0.741	0.854	0.756	0.923	0.697
35%	0.881	0.741	0.977	0.760	0.888	0.775	0.967	0.772	0.881	0.766	0.962	0.758	0.886	0.800	0.947	0.765	0.862	0.776	0.922	0.713
30%	0.888	0.757	0.979	0.775	0.896	0.785	0.972	0.787	0.890	0.781	0.966	0.776	0.894	0.811	0.951	0.781	0.867	0.787	0.922	0.723
25%	0.892	0.765	0.981	0.782	0.900	0.798	0.970	0.795	0.905	0.809	0.971	0.805	0.900	0.821	0.956	0.795	0.879	0.806	0.930	0.749
20%	0.906	0.800	0.980	0.810	0.910	0.813	0.977	0.817	0.905	0.810	0.972	0.806	0.910	0.844	0.955	0.812	0.885	0.823	0.928	0.760

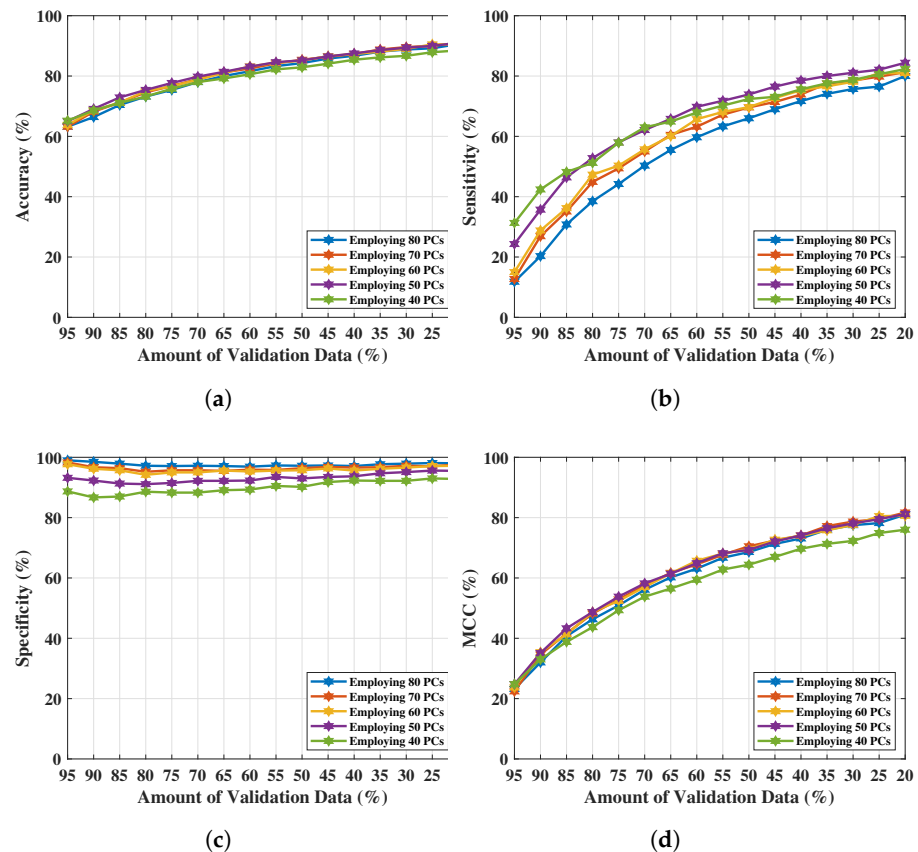


Figure 8. NF and WF signal classification results obtained from SVM_G applying PCA over real-parts of MammoWave’s complex S_{21} data. (a) Accuracy obtained from SVM_G varying PCs and validation data. (b) Sensitivity obtained from SVM_G varying PCs and validation data. (c) Specificity obtained from SVM_G varying PCs and validation data. (d) MCC obtained from SVM_G varying PCs and validation data.

NF-WF signal classification has been performed with the PCs extracted from $\lambda_{real}(n)$ (up to 80 PCs) and executing SVM_G for breast lesion identification. Classification results have been tabulated in Table 9, where A_c , S_e , S_p , and MCC are presented with varying number of PCs (interval of 10 units). The optimal classification performance was achieved with 50 PCs, but begins to decrease upon further reduction (i.e., 40 PCs). The resultant metrics are plotted in Figure 8a–d for comparison between each metric with the PCs variation. Metrics, A_c , S_e , S_p , and MCC increased from 90.90% to 91%, 84.30% to 84.40%, 95.30% to 95.50%, and 81% to 81.20% respectively using the PCs ($\sigma_1, \sigma_2, \dots, \sigma_{50}$) extracted from $\lambda_{real}(n)$ instead of the PCs extracted from $\lambda_n = \sum_{n=1}^{NF=1601} \lambda_{real}(n) + j\lambda_{img}(n)$. Classification performance improved from the performance achieved in Section 4.1, signifying that PCs derived from resistance components are more enlightening than PCs derived from both S_{21} resistance and reactance components to represent NF-WF breast signals (as well as the NF-WF breasts). Hence, the performance obtained from 50 PCs with SVM_G is considered as the optimal validation classification performance. Further two parameters; regularisation and scaling parameter have been tuned to search the space of possible hyperparameter values that results optimum validation results of the proposed model. The regularisation parameter 1 found to be optimal while the model is noticed to be reactive to the variation of kernel scale. Therefore, the ROC curve has been calculated varying kernel scaling parameter to select optimal value, displayed in Figure 9 and measured the area under the ROC curve ($AUC = 0.99$). The x and y-axes of Figure 9 represents false positive rate (FPR) or (1-specificity) and true positive rate (TPR) or sensitivity respectively. The threshold of ROC curve has been found to be kernel scaling parameter 1.8 for locating the balanced true and false positive rates. Hence, the optimal results $A_c = 95.07\%$, $S_e = 92.40\%$, $S_p = 98.32\%$,

and $MCC = 89.90\%$ for validation performance have been decided considering kernel scaling parameter 1.8.

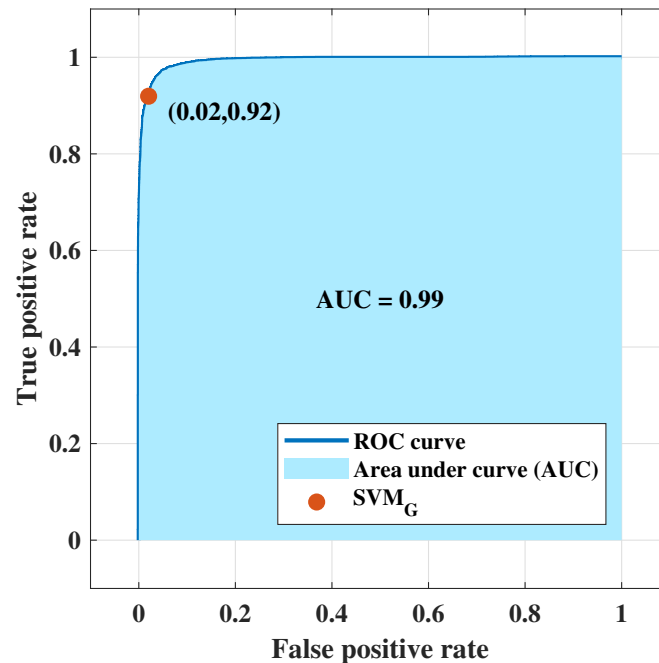


Figure 9. ROC curve obtained from SVM_G employing principal components of real parts of S_{21} signals for NF-WF signal classification.

4.4. Classification Applying Optimal Settings: Training, Validation, Testing Experiment

Once the training and validation process have been completed that apprise the 50 PCs extracted from real parts of complex S_{21} are most efficient for classifying NF and WF signals among all the feature extraction combination employed before. The experiment has now reorganised with the data broken into training, validation, and testing set for addressing data contamination and realise the final unbiased model performance on truly unseen test data set. Table 10 demonstrates the final performance obtained in the proposed work. As limited number of breasts (61 breasts' data) are available at this stage of research, 20% (12 randomly selected breasts), 25% (15 randomly selected breasts) data have been stratified and held-out using MCCV procedure as test set initially. Rest of the 80%, 75% data have been used for training-validation process using optimal number of 50 PCs of real parts and applying SVM_G on 80% allocated training and 20% validation, as settled in Section 4.3. Same performance metrics accuracy, sensitivity, specificity, and MCC have been calculated to analyse the performance. It is found that, the trained and validated SVM_G model with 50 PCs of real parts of complex S_{21} outperforms in 20% testing dataset (and 80% training-validation set). The attained performance includes the accuracy $A_c = 95.50\%$, sensitivity $S_e = 97.20\%$, specificity $S_p = 94.50\%$, and $MCC = 90.90\%$, whereas the metrics were $A_c = 95.00\%$, $S_e = 92.40\%$, $S_p = 98.30\%$, and $MCC = 89.90\%$ before.

Table 10. Training, validation, and testing dataset: classification results applying PCs extracted from real parts of MammoWave's complex S_{21} signals with SVM_C .

Total Breasts	Training-Validation Data	Training Data	Validation Data	Feature Dimension PC-50				Testing Data	Feature Dimension PC-50			
				A_c	S_e	S_p	MCC		A_c	S_e	S_p	MCC
61 Breasts	75% of Data (46 Breasts)	80%	20%	84.20%	88.20%	82.20%	67.40%	25% of Data (15 breasts)	94.40%	96.20%	93.40%	88.50%
61 Breasts	80% of Data (49 Breasts)	80%	20%	85.40%	88.80%	83.60%	69.70%	20% of Data (12 breasts)	95.50%	97.20%	94.50%	90.90%

5. Discussion & Conclusions

The proposed methodology have three primary focuses: (1) the absence of radiation exposure through MammoWave have many potential benefits compared to the mammography; specifically, women will benefit from safe and accessible radiation-free breast cancer screening, more inclusive (no age-limitation), and more comfortable (no breast compression), (2) the study is part of a retrospective clinical trials, (3) the embrace of robust machine learning models using microwave breast imaging, makes it a cutting edge solution for safe breast lesions detection.

The structure of proposed support vector machine is simple to interpret and performed flexibly with the data. Proposed research outperformed with statistically and biologically dependent data as signals are generated and transmitted using same frequency band for each breast scanning and each patient's body responds differently to microwave signal transmission. The signal data are fused while preparing for ML application. The procedure is computationally less complex and fast. Results are cross validated using MCCV method. Therefore, the proposed research is protected from several limitations. The experiment in [39] showed that breast frequency response is discriminative and independent where quadratic kernel of SVM can differentiate the signal response reflected from NF and WF breasts with acceptable sensitivity and specificity. However, in [39], SVM_Q was applied on a limited number of patients after performing a dedicated S_{21} pre-processing for artefact removal. The proposed work aims to provide a quantitative portrayal of NF-WF breast classification through MammoWave applying the ML algorithm directly to the raw S_{21} , i.e., raw-data. In this scenario, it has been found that SVM_G outperformed SVM_Q . Specifically, SVM_G was executed on the NF-WF signals of 61 breasts from 35 patients who participated in the feasibility clinical trial, showing satisfactory and improved prediction performance. Accuracy > 91%, sensitivity > 84%, specificity > 95%, and MCC > 81% were achieved through this study. Hence, this proposed study attained remarkable performance in the task of identifying or separating NF and WF (or lesion) signals automatically from raw signal data. The achieved sensitivity (84.40%) and specificity (95.50%) are similar to digital mammography sensitivity [44,45]. However, the MammoWave breast screening is non-invasive and painless and can be used across all ages, during pregnancy and multiple times.

The sensitivity value aligns with the MARIA system which has been used in symptomatic patients [24,25]. The MARIA system (Micrima Ltd, UK) uses an array of 60 antennas and a matching liquid to carry out the radar approach), which is far more complex than the one presented here. The proposed classification algorithm predicted false negatives (actually WF but predicted as NF) in some cases, effecting the sensitivity (84.40%) measure. This was due to the presence of very small sized lesion (few mm or smaller). There are low differences found between the signals value of NF and WF breasts with very small sized lesions. Therefore, numerically NF breasts and WF breasts with very small sized lesion behave similarly, misguiding the classification process, resulting in false negative predictions. This issue will be addressed in our future work by modifying the conventional SVM_G kernel structure and performing advance research on feature representation. Moreover, we will investigate the use of microwave image features [22] for dedicated machine learning models, following a procedure similar to [46], where the authors used radiomics derived from Contrast-Enhanced Spectral Mammography Images, obtaining a sensitivity and specificity of 88.37% and 100%.

Raw scan of each breast contains 1200 complex S_{21} signals. Classification of NF-WF signals with high specificity and sensitivity will help to decide the threshold for a breast to be entitled as NF or WF which will help to determine further clinical procedure for the patients. The research for detecting the threshold is underway. Also, further research and more breast data are required to generalise that threshold for breast classification because, a main limitation of the study is represented by the fact that a limited number of breast has been used. Research is in progress using data collected in other MammoWave clinical trials, just ended (<https://clinicaltrials.gov/ct2/show/NCT04253366>). In this circumstance, ML

study will be carried on with ongoing MammoWave clinical trial data [47]. Moreover, further clinical trials are planned to enlarge the resulting research database [48], paving the way for the use of microwave imaging into clinical practice as complementary tool for the screening of asymptomatic women of any age and without any safety restrictions. It is worthwhile pointing out that one of the goals of HORIZON-MISS-2021-CANCER-02-01 scheme is to validate new methods and technologies for cancer screening and early detection, preferably non-invasive and more-inclusive than current approaches. In this context, one of the selected projects has the aim of generating evidence on thousands of women regarding the use of MammoWave as breast cancer screening technique [48].

Author Contributions: G.T. and the team have designed and manufactured the UWB microwave non-ionising apparatus with associated signal processing techniques comprising MammoWave. Subjects have been recruited and screened through MammoWave. R.L. and M.D. (Michele Duranti) have conducted the conventional radiological investigation on the same subjects and confirmed the outcomes of UWB MammoWave experiment. S.P.R. analysed, interpreted the data for ML application, performed the ML algorithms, and made the draft. S.P.R. and M.D. (Maitreyee Dey) have analysed the prediction outcomes for automatic breast lesion detection through clinical UWB MammoWave. S.D. and G.T. have supervised the work and managed the experiments performed along with the co-authors at LSBU. S.D., G.T. and M.G. instigated the collaborative work on this paper between the teams at UBT, Perugia and LSBU. All authors have read and agreed to the published version of the manuscript.

Funding: This project has received funding from the European Union’s Horizon 2020 research and innovation programme under grant agreement No 830265. This project leading to this application has received funding from the European Union’s Horizon 2020 research and innovation programme under the Marie Skłodowska-Curie grant agreement No. 793449. This project has received funding from the European Union’s Horizon 2020 research and innovation programme under the Marie Skłodowska-Curie grant agreement No. 872752.

Institutional Review Board Statement: The protocol and procedures were conducted in accordance with institutional and ethical standards in research, with Declaration of Helsinki (1964) and its later amendments. The MammoWave feasibility clinical validation has been performed in Perugia and Foligno Hospitals, Italy (Ethical Committee of Umbria, Italy, approval N. 6845/15/AV/DM of 14/10/2015, N. 10352/17/NCAV of 16/03/2017, N 13203/18/NCAV of 17/04/2018).

Informed Consent Statement: Prior to the trial, informed consent was obtained from all participants involved in the study.

Data Availability Statement: The datasets that support the findings of this study are not publicly available, but will be made available upon reasonable request, following ethics committee approval and a data transfer agreement to guarantee the General Data Protection Regulation. Please contact the authors, Soumya Prakash Rana (Email: ranas11@lsbu.ac.uk, soumyaparakash.rana@gmail.com) or Gianluigi Tiberi (Email: tiberig@lsbu.ac.uk, gianluigi@ubt-tech.com) to request access to the data.

Conflicts of Interest: Gianluigi Tiberi is shareholders of UBT—Umbria Bioengineering Technologies. This does not alter our adherence to MDPI journal policies on sharing data and materials.

References

1. Yedjou, C.G.; Sims, J.N.; Miele, L.; Noubissi, F.; Lowe, L.; Fonseca, D.D.; Alo, R.A.; Payton, M.; Tchounwou, P.B. Health and racial disparity in breast cancer. In *Breast Cancer Metastasis Drug Resistance*; Springer: Basel, Switzerland, 2019, pp. 31–49.
2. Miglioretti, D.L.; Lange, J.; Van Den Broek, J.J.; Lee, C.I.; Van Ravesteyn, N.T.; Ritley, D.; Kerlikowske, K.; Fenton, J.J.; Melnikow, J.; De Koning, H.J.; et al. Radiation-induced breast cancer incidence and mortality from digital mammography screening: A modeling study. *Ann. Intern. Med.* **2016**, *164*, 205–214. [[CrossRef](#)] [[PubMed](#)]
3. Seiffert, K.; Thoene, K.; Zu Eulenburg, C.; Behrens, S.; Schmalfeldt, B.; Becher, H.; Chang-Claude, J.; Witzel, I. The effect of family history on screening procedures and prognosis in breast cancer patients—Results of a large population-based case-control study. *Breast* **2021**, *55*, 98–104. [[CrossRef](#)] [[PubMed](#)]
4. Miller, A.M.; Champion, V.L. Attitudes about breast cancer and mammography: Racial, income, and educational differences. *Women Health* **1997**, *26*, 41–63. [[CrossRef](#)]
5. Loving, V.A.; Aminololama-Shakeri, S.; Leung, J.W. Anxiety and its association with screening mammography. *J. Breast Imaging* **2021**, *3*, 266–272. [[CrossRef](#)]

6. Tiberi, G.; Raspa, G. Apparatus for Testing the Integrity of Mammary Tissues. US Patent 10,349,863, 2019.
7. Sensitivity, Specificity, and False Negative Rate for 1,682,504 Screening Mammography Examinations from 2007–2013. In *Technical Report*; Breast Cancer Surveillance Consortium (BCSC): Seattle, WA, USA, 2017.
8. Stout, N.K.; Lee, S.J.; Schechter, C.B.; Kerlikowske, K.; Alagoz, O.; Berry, D.; Buist, D.S.; Cevik, M.; Chisholm, G.; De Koning, H.J.; et al. Benefits, harms, and costs for breast cancer screening after US implementation of digital mammography. *JNCI: J. Natl. Cancer Inst.* **2014**, *106*, dju092. [[CrossRef](#)] [[PubMed](#)]
9. Nelson, H.D.; Pappas, M.; Cantor, A.; Griffin, J.; Daeges, M.; Humphrey, L. Harms of breast cancer screening: Systematic review to update the 2009 US Preventive Services Task Force recommendation. *Ann. Intern. Med.* **2016**, *164*, 256–267. [[CrossRef](#)]
10. Fanizzi, A.; Basile, T.; Losurdo, L.; Amoroso, N.; Bellotti, R.; Bottigli, U.; Dentamaro, R.; Didonna, V.; Fausto, A.; Massafra, R.; et al. Hough transform for clustered microcalcifications detection in full-field digital mammograms. In *Applications of Digital Image Processing XL*; International Society for Optics and Photonics: San Diego, California, United States, 2017, Volume 10396, p. 1039616.
11. Bibault, J.E.; Giraud, P.; Burgun, A. Big data and machine learning in radiation oncology: State of the art and future prospects. *Cancer Lett.* **2016**, *382*, 110–117. [[CrossRef](#)]
12. Zhang, B.; He, X.; Ouyang, F.; Gu, D.; Dong, Y.; Zhang, L.; Mo, X.; Huang, W.; Tian, J.; Zhang, S. Radiomic machine-learning classifiers for prognostic biomarkers of advanced nasopharyngeal carcinoma. *Cancer Lett.* **2017**, *403*, 21–27. [[CrossRef](#)]
13. Huang, S.; Yang, J.; Fong, S.; Zhao, Q. Artificial intelligence in cancer diagnosis and prognosis: Opportunities and challenges. *Cancer Lett.* **2020**, *471*, 61–71. [[CrossRef](#)]
14. McKinney, S.M.; Sieniek, M.; Godbole, V.; Godwin, J.; Antropova, N.; Ashrafian, H.; Back, T.; Chesus, M.; Corrado, G.S.; Darzi, A.; et al. International evaluation of an AI system for breast cancer screening. *Nature* **2020**, *577*, 89–94. [[CrossRef](#)]
15. Hickman, S.E.; Baxter, G.C.; Gilbert, F.J. Adoption of artificial intelligence in breast imaging: Evaluation, ethical constraints and limitations. *Br. J. Cancer* **2021**, *125*, 15–22. [[CrossRef](#)] [[PubMed](#)]
16. Meaney, P.M.; Fanning, M.W.; Raynolds, T.; Fox, C.J.; Fang, Q.; Kogel, C.A.; Poplack, S.P.; Paulsen, K.D. Initial clinical experience with microwave breast imaging in women with normal mammography. *Acad. Radiol.* **2007**, *14*, 207–218. [[CrossRef](#)] [[PubMed](#)]
17. Bahrami Barghouei, H.; Porter, E.; Santorelli, A.; Gosselin, B.; Popović, M.; Rusch, L.A. Flexible 16 antenna array for microwave breast cancer detection. *IEEE Trans. Biomed. Eng.* **2015**, *62*, 2516–2525. [[CrossRef](#)]
18. Bond, E.J.; Li, X.; Hagness, S.C.; Van Veen, B.D. Microwave imaging via space-time beamforming for early detection of breast cancer. *IEEE Trans. Antennas Propag.* **2003**, *51*, 1690–1705. [[CrossRef](#)]
19. Fear, E.C.; Li, X.; Hagness, S.C.; Stuchly, M.A. Confocal microwave imaging for breast cancer detection: Localization of tumors in three dimensions. *IEEE Trans. Biomed. Eng.* **2002**, *49*, 812–822. [[CrossRef](#)]
20. Meaney, P.M.; Fanning, M.W.; Li, D.; Poplack, S.P.; Paulsen, K.D. A clinical prototype for active microwave imaging of the breast. *IEEE Trans. Microw. Theory Tech.* **2000**, *48*, 1841–1853.
21. O’Loughlin, D.; O’Halloran, M.; Moloney, B.M.; Glavin, M.; Jones, E.; Elahi, M.A. Microwave breast imaging: Clinical advances and remaining challenges. *IEEE Trans. Biomed. Eng.* **2018**, *65*, 2580–2590. [[CrossRef](#)]
22. Sani, L.; Vispa, A.; Loretoni, R.; Duranti, M.; Ghavami, N.; Alvarez Sánchez-Bayuela, D.; Caschera, S.; Paoli, M.; Bigotti, A.; Badia, M.; et al. Breast lesion detection through MammoWave device: Empirical detection capability assessment of microwave images’ parameters. *PLoS ONE* **2021**, *16*, e0250005. [[CrossRef](#)]
23. Meaney, P.M.; Kaufman, P.A.; Muffly, L.S.; Click, M.; Poplack, S.P.; Wells, W.A.; Schwartz, G.N.; di Florio-Alexander, R.M.; Tosteson, T.D.; Li, Z.; et al. Microwave imaging for neoadjuvant chemotherapy monitoring: Initial clinical experience. *Breast Cancer Res.* **2013**, *15*, 1–16. [[CrossRef](#)]
24. Preece, A.W.; Craddock, I.; Shere, M.; Jones, L.; Winton, H.L. MARIA M4: Clinical evaluation of a prototype ultrawideband radar scanner for breast cancer detection. *J. Med Imaging* **2016**, *3*, 033502. [[CrossRef](#)]
25. Massey, H.; Ridley, N.; Lyburn, I.; Taylor, S.; Schoenleber-Lewis, M.; Bannister, P.; Shere, M.H. Radio-wave detection of breast cancer in the symptomatic clinic—a multi-centre study. In *Proceedings of the International Cambridge Conference on Breast Imaging*, Cambridge, UK, 3–4 July 2017; pp. 3–4.
26. Curtis, C.; Lavoie, B.R.; Fear, E. An analysis of the assumptions inherent to near-field beamforming for biomedical applications. *IEEE Trans. Comput. Imaging* **2017**, *3*, 953–965. [[CrossRef](#)]
27. Yang, F.; Sun, L.; Hu, Z.; Wang, H.; Pan, D.; Wu, R.; Zhang, X.; Chen, Y.; Zhang, Q. A large-scale clinical trial of radar-based microwave breast imaging for Asian women: Phase I. In *Proceedings of the 2017 IEEE International Symposium on Antennas and Propagation & USNC/URSI National Radio Science Meeting*, San Diego, CA, USA, 9–14 July 2017; pp. 781–783.
28. Kurrant, D.; Bourqui, J.; Fear, E. Surface estimation for microwave imaging. *Sensors* **2017**, *17*, 1658. [[CrossRef](#)] [[PubMed](#)]
29. Song, H.; Sasada, S.; Kadoya, T.; Okada, M.; Arihiro, K.; Xiao, X.; Kikkawa, T. Detectability of breast tumor by a hand-held impulse-radar detector: performance evaluation and pilot clinical study. *Sci. Rep.* **2017**, *7*, 1–11. [[CrossRef](#)]
30. Porter, E.; Duff, K.; Popovic, M.; Coates, M. Investigation of time-domain microwave radar with breast clinic patients. In *Proceedings of the 2016 10th European Conference on Antennas and Propagation (EuCAP)*, Davos, Switzerland, 10–15 April 2016; pp. 1–3.
31. Kuwahara, Y.; Malik, A. Microwave imaging for early breast cancer detection. *New Perspectives Breast Imaging*; IntechOpen: London, UK, 2017; pp. 45–71.

32. Ghavami, N.; Tiberi, G.; Edwards, D.J.; Monorchio, A. UWB microwave imaging of objects with canonical shape. *IEEE Trans. Antennas Propag.* **2011**, *60*, 231–239. [[CrossRef](#)]
33. Tiberi, G.; Sani, L.; Ghavami, N.; Paoli, M.; Vispa, A.; Raspa, G.; Vannini, E.; Saracini, A.; Duranti, M. Sensitivity assessment of a microwave apparatus for breast cancer detection. In Proceedings of the European Congress of Radiology-ECR 2018, Vienna, Austria, 28 February–4 March 2018.
34. Da Silva, D.; Kaduri, M.; Poley, M.; Adir, O.; Krinsky, N.; Shainsky-Roitman, J.; Schroeder, A. Biocompatibility, biodegradation and excretion of polylactic acid (PLA) in medical implants and theranostic systems. *Chem. Eng. J.* **2018**, *340*, 9–14. [[CrossRef](#)]
35. Sani, L.; Ghavami, N.; Vispa, A.; Paoli, M.; Raspa, G.; Ghavami, M.; Sacchetti, F.; Vannini, E.; Ercolani, S.; Saracini, A.; et al. Novel microwave apparatus for breast lesions detection: Preliminary clinical results. *Biomed. Signal Process. Control* **2019**, *52*, 257–263. [[CrossRef](#)]
36. Lazebnik, M.; Popovic, D.; McCartney, L.; Watkins, C.B.; Lindstrom, M.J.; Harter, J.; Sewall, S.; Ogilvie, T.; Magliocco, A.; Breslin, T.M.; et al. A large-scale study of the ultrawideband microwave dielectric properties of normal, benign and malignant breast tissues obtained from cancer surgeries. *Phys. Med. Biol.* **2007**, *52*, 6093. [[CrossRef](#)]
37. Conceição, R.C.; Mohr, J.J.; O'Halloran, M. *An Introduction to Microwave Imaging for Breast Cancer Detection*; Springer: Basel, Switzerland, 2016.
38. Noble, W.S. What is a support vector machine. *Nat. Biotechnol.* **2006**, *24*, 1565–1567. [[CrossRef](#)]
39. Rana, S.P.; Dey, M.; Tiberi, G.; Sani, L.; Vispa, A.; Raspa, G.; Duranti, M.; Ghavami, M.; Dudley, S. Machine learning approaches for automated lesion detection in microwave breast imaging clinical data. *Sci. Rep.* **2019**, *9*, 1–12. [[CrossRef](#)]
40. He, Q.; Kong, F.; Yan, R. Subspace-based gearbox condition monitoring by kernel principal component analysis. *Mech. Syst. Signal Process.* **2007**, *21*, 1755–1772. [[CrossRef](#)]
41. Xu, Q.S.; Liang, Y.Z. Monte Carlo cross validation. *Chemom. Intell. Lab. Syst.* **2001**, *56*, 1–11. [[CrossRef](#)]
42. Powers, D.M. Evaluation: From precision, recall and F-measure to ROC, informedness, markedness and correlation. *arXiv* **2020**, arXiv:2010.16061.
43. Matthews, B.W. Comparison of the predicted and observed secondary structure of T4 phage lysozyme. *Biochim. Et Biophys. Acta (BBA)-Protein Struct.* **1975**, *405*, 442–451. [[CrossRef](#)]
44. Pisano, E.D.; Hendrick, R.E.; Yaffe, M.J.; Baum, J.K.; Acharyya, S.; Cormack, J.B.; Hanna, L.A.; Conant, E.F.; Fajardo, L.L.; Bassett, L.W.; et al. Diagnostic accuracy of digital versus film mammography: Exploratory analysis of selected population subgroups in DMIST. *Radiology* **2008**, *246*, 376–383. [[CrossRef](#)]
45. Zeeshan, M.; Salam, B.; Khalid, Q.S.B.; Alam, S.; Sayani, R. Diagnostic accuracy of digital mammography in the detection of breast cancer. *Cureus* **2018**, *10*. [[CrossRef](#)]
46. Massafra, R.; Bove, S.; Lorusso, V.; Biafora, A.; Comes, M.C.; Didonna, V.; Diotaiuti, S.; Fanizzi, A.; Nardone, A.; Nolasco, A.; et al. Radiomic Feature Reduction Approach to Predict Breast Cancer by Contrast-Enhanced Spectral Mammography Images. *Diagnostics* **2021**, *11*, 684. [[CrossRef](#)]
47. ClinicalTrials.gov. 2020. Available online: <https://clinicaltrials.gov/ct2/show/NCT04253366> (accessed on 24 August 2021).
48. Tiberi, G. Presenting MammoScreen project: Innovative and safe microwave-based imaging technology to make breast cancer screening more accurate, inclusive, and female-friendly, ECR 2023, RPS 702, Advanced applications in breast imaging, 2023, Vienna, Austria on March 1–5, 2023. (*Just accepted*).

Disclaimer/Publisher's Note: The statements, opinions and data contained in all publications are solely those of the individual author(s) and contributor(s) and not of MDPI and/or the editor(s). MDPI and/or the editor(s) disclaim responsibility for any injury to people or property resulting from any ideas, methods, instructions or products referred to in the content.